Microtopography, water storage and flow patterns in a fine-textured soil under agricultural use

Christina Bogner, Mohammadreza Mirzaei, Stéphane Ruy, Bernd Huwe

Microtopography, water storage and flow patterns in a fine-textured soil under agricultural use

Christina Bogner*[1], Mohammadreza Mirzaei[2], Stéphane Ruy[3], and Bernd Huwe[4]

[1]*Ecological Modelling, BayCEER, University of Bayreuth, Dr.-Hans-Frisch-Straße 1–3, 95448 Bayreuth, Germany*
[2]*Faculty of Agriculture, Natural Resources and Environment Institute, Yaouj University, Yasouj, I.R. Iran*
[3]*UMR EMMAH, INRA, Domaine St Paul – Agroparc, 84914 Avignon Cedex 9, France*
[4]*Soil Physics Group, BayCEER, University of Bayreuth, 95440 Bayreuth, Germany*

Abstract

Agricultural use of soils implies tillage and often compaction and therefore influences processes on soil surface and affects infiltration of water into the subsoil. While many studies on soil surface processes or flow patterns in soils exist, works relating both are rare in literature. We did two tracer experiments with Brilliant Blue FCF on a tilled and compacted plot and a non-tilled one to investigate water storage on the soil surface during simulated rainfall and changes of soil microtopography, to analyse the associated flow patterns in the soil and to relate both to tillage and compaction. Our results show that storage was larger on the tilled and compacted plot than on the non-tilled one. After tillage, transport processes above the plough pan were partly disconnected from those underneath because macropores were disrupted and buried by the tillage operation. However, preferential flow along cracks occurred on both plots and macropores buried below the tillage pan still functioned as preferential flow paths. Therefore, we conclude that the studied soil is susceptible to deep vertical solute propagation at dry conditions when cracks are open, irrespective of tillage and compaction.

Keywords: agricultural soils; soil microtopography; surface water storage; dye tracers; preferential flow; flow patterns

*Correspondence to: Christina Bogner, BayCEER, University of Bayreuth, Dr.-Hans-Frisch-Straße 1–3, 95448 Bayreuth, Germany.
E-mail: christina.bogner@uni-bayreuth.de
This is an author's post-print version of the article published in Hydrological Processes, **27**, 1797–1806 (2012) doi:10.1002/hyp.933

1 Introduction

The surface of agricultural soils is subjected to frequent changes by tillage. Tillage operations influence the microtopography and modify the surface roughness of soils, where roughness is a measure of variations of soil microtopography (Huang, 1998). Several important processes depend on soil microtopography: infiltration, water storage in depressions, erosion and sedimentation, to name but a few. Rough soil surfaces, for instance, tend to store more water thus reducing runoff and increasing infiltration (Hairsine et al., 1992; Hansen et al., 1999).

Many techniques have been used to measure soil surface microtopography, ranging from a simple roller chain to a laser scanner (see Jester and Klik, 2005, for an overview). Stereo photogrammetry is a relatively recent method that allows rapid data acquisition under field conditions. Taconet and Ciarletti (2007), for example, reported that stereo photogrammetry systems could be used in hydraulic and erosion studies and provided accurate estimation of soil digital elevation models (DEMs).

During tillage operations, compaction of the soil might occur as a result of the employment of heavy machinery. In modern agriculture, compaction has become an important issue because it reduces soil porosity (especially macroporosiy) and might decrease crop yields (Alakukku, 1996a; Håkansson and Reeder, 1994). While in the topsoil tillage counterbalances the effect of compaction, it could persist for several years in the subsoil (Alakukku, 1996b).

Besides its effect on soil microtopography, tillage is known to affect the pore system and hydraulic properties of the soil (e.g Strudley et al., 2008; Tebrugge and During, 1999) and thus to influence infiltration and water flow at least in the topsoil. Once infiltrated, water often moves along preferential flow paths through the soil and can bypass a large portion of the soil matrix (Hendrickx and Flury, 2001). This preferential flow is closely related to soil structure (Ghodrati and Jury, 1992; Vervoort et al., 1999) whose alteration by tillage might strongly affect flow processes.

In soil hydrology, water flow is often visualised in tracer studies by the food dye Brilliant Blue FCF (Flury et al., 1994; Pickering et al., 1988). This tracer has the advantage of good visibility against most soil colours and acceptable toxicological properties for environmental use (Flury and Flühler, 1994). Using this dye Kulli et al. (2003), for example, showed that soil compaction due to employment of heavy machinery modified the pore system by degrading or destroying the soil structure. As a consequence, soil mechanical parameters like bulk density were changed and the transport properties of the pore system were modified.

Many studies analysing the impact of tillage or compaction on soil surface microrelief (e.g. Moreno et al., 2008; Paz-Ferreiro et al., 2008; Vidal Vàzquez et al., 2006) or on flow patterns exist (e.g. Kulli et al., 2003; Mooney and Nipattasuk, 2003). However, to our knowledge, works relating processes on the soil surface with associated flow patterns are rare in literature. Our study aims to combine stereo photogrammetry with dye staining technique to investigate (i) water storage on the soil surface during simulated rainfall and (ii) changes in microtopography; (iii) to analyse the associated flow patterns in the soil and (iv) to relate both to tillage and compaction. A special emphasis will be given to the coupling of infiltration processes above and below the plough pan. Finally, we will give (v) an evaluation of the susceptibility of the studied soil to vertical solute propagation.

Table 1: Particle size distribution (without decarbonisation) of the soil fine fraction analysed by laser diffraction. Sand fraction is defined as 2000–63 µm, silt 63–2 µm and clay < 2 µm.

Plot	Depth (cm)	Sand (%)	Silt (%)	Clay (%)
I	10-26	6.37	47.70	45.94
	26-56	5.00	47.59	47.41
	56-100	15.98	46.36	37.66
II	0-30	5.18	48.35	46.47
	30-60	4.94	48.14	46.93
	60-100	15.53	47.63	36.85

2 Materials and methods

2.1 Dye tracer experiments

The research area is situated on an alluvial plane at about 30 m above sea level at the confluence of Rhone and Durance rivers in South France. Here, the river deposits constitute an important aquifer with a shallow water table that can rise up to 3 m below the surface. The study site is an agricultural field planted with wheat and located at the experimental domain of INRA Avignon (43°54′58.76″N, 4°52′54.81″E). The soil is a highly structured Calcisol (IUSS Working Group WRB, 2007) with a pH_{H_2O} of 8.5 and an important content of clay (Table 1). The latter is responsible for the development of deep cracks in the soil during desiccation.

We did two rainfall simulation experiments with a tracer solution containing $5\,g\,l^{-1}$ Brilliant Blue FCF (a sodium salt) and $5\,g\,l^{-1}$ potassium iodide. This solution was evenly irrigated at $64\,mm\,hour^{-1}$ on a surface of about $1\,m^2$ during one hour with an automated sprinkler similar to that described by Ghodrati et al. (1990). In order to keep the infiltrated volume of tracer solution comparable between plots, we installed a metallic frame around the plots to avoid large runoff. Several previous works (e.g. German-Heins and Flury, 2000; Ketelsen and Meyer-Windel, 1999) showed that Brilliant Blue was sorbed by soil particles and thus might be considerably retarded with regard to infiltrating water. Therefore, we used potassium iodide as a reference tracer to be sure that Brilliant Blue infiltration patterns reflected well those of water.

For the first experiment the wheat was harvested and the soil surface was tilled with a plough share followed by a circular spike harrow combined with a cultipacker. Subsequently, the middle part of the plot was compacted by repeated passage of a tractor wheel. This plot was slightly inclined and had a slope going from the left upper corner to the right lower part (Figure 1a). The day before tracer application we did a preliminary rainfall simulation on this plot with 56 mm of water without tracer to test the stereo system. In contrast, the surface of plot two was not tilled, but the wheat was cut before tracer application. We have chosen plot two for its well developed open fissures (Figure 1b). Indeed, such cracks were visible all over the field and plot two was therefore representative for the natural surface and moisture conditions.

During the rainfall simulation we monitored the storage of the tracer solution on the soil

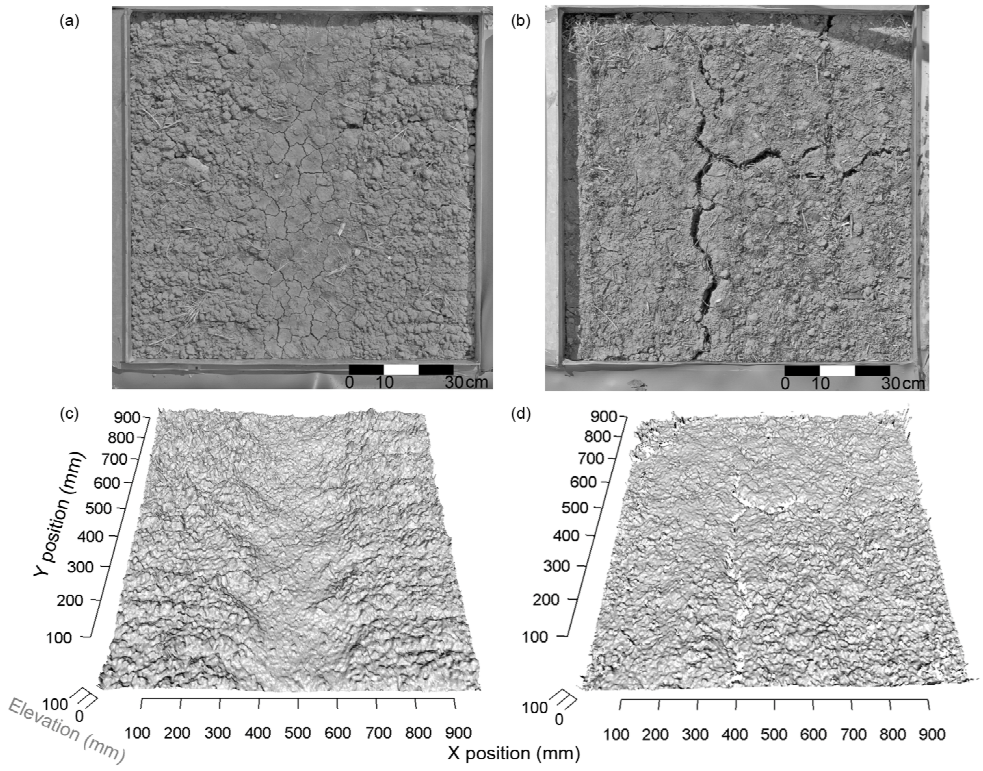

Figure 1: Soil surface before dye tracer application with a compacted middle part on plot one (a) and with a well developed system of open cracks on plot two (b); DEM of plot one (c) and of plot two (d). The surface of plot one was inclined with a general slope from the left upper corner to the right lower corner of the plot. In contrast, the surface of plot two was generally flat. The supplementary online material contains coloured photographs of the soil surface and the DEMs in higher resolution.

surface by a stereo system consisting of two Nikon D100 cameras installed in approximately 3 m height (Mirzaei, 2008). Additionally, we measured soil moisture with TDR (Time Domain Reflectometry) probes. On plot one, two TDR probes were placed in 8 and 18 cm depth in the compacted and tilled parts of the plot, respectively. On plot two, 11 probes were installed: four in 8 and 15 cm and three in 30 cm depth, respectively. Nine of these probes were situated in the soil matrix and three in cracks. The TDR probes inserted into the cracks at 8 and 15 cm depth were placed in the wall of a crack. In contrast, the TDR probe installed in 30 cm was located at the bottom of a fissure inside loose soil material and captured the dynamics of water circulating inside the cracks. The probes were inserted from a small trench opened at the upper limit of the plots (Figure 1a).

The day after tracer application we prepared vertical soil profiles of 1 m $\times$ 1 m (10 on plot one and 11 on plot two) and photographed them with a digital CCD camera. The soil profiles looked distorted on the photographs because the camera could not be positioned exactly perpendicularly to the profile. Moreover, the illumination varied during the day and the same colours appeared differently in the morning compared to evening images. Therefore, we used a metallic frame of 1 m^2 that defined the part of the soil profile we wanted to analyse

and two Kodak reference grey scales and photographed them with the soil profiles. This frame and the grey scales were used for geometric correction and white balance adjustment.

To verify that Brilliant Blue patterns corresponded well to those of infiltrating water, we treated two profiles per plot with an indicator solution of iron(III) nitrate and starch (Lu and Wu, 2003). Iodide is supposed to reduce iron(III) and to react to iodine that builds a violet complex with starch. This color then indicates iodide infiltration patterns. However, in our experiment the colour reaction failed to appear probably because of large pH values in the soil. Indeed, the reduction potential of the iodide-iodine system is only independent of the pH as long as the latter remains less than 8. For larger pH values (at our study site the pH_{H_2O} was 8.5) iodine reacts with hydroxide ions to iodate and iodide (Jeffery et al., 1989, p. 385) so that the iodine-starch complex is not built.

2.2 Image analysis

2.2.1 Stereo images of the soil surface

The stereo system produced images of the soil surface from two different points of view (stereo images). These images were matched point by point to calculate a DEM of the soil surface (e.g. Jeschke, 1990; Warner, 1995). In his work, Mirzaei (2008) gives a detailed description of the procedure. The DEM was the basis to determine the stored volume of the tracer and the area covered by puddles during the experiment. According to the calibration procedure and the geometry of the device (soil-camera distance: 3 m, focal length: 0.04 m, distance between the cameras: 0.4 m) the horizontal resolution of the DEMs was 0.4 mm^2 and its vertical 0.6 mm.

The point matching process produced noisy data or missing values close to the metallic frame and in areas shaded by soil clods because of occlusion or a poor contrast. Additionally, wheat residues on the surface of plot two gave particularly large elevations that were not due to the structure of the soil surface. In contrast, cracks produced missing values or particularly small elevations. These problems are typical for the stereo photogrammetry. Jester and Klik (2005), for instance, identified steep surface slopes and shadowed voids as main error sources for DEM calculation. The matching of stereo images and calculation of DEMs were implemented in HALCON (MVTec Software GmbH, Munich, Germany).

2.2.2 Stored volume and area covered by puddles

The point matching process was especially poor along frame walls. Thus, for calculations of the stored volume and the area covered by puddles we only analysed the inner 0.94 m^2 of the surface and ignored puddles along frame walls. Furthermore, the DEM had missing values that we had to fill by gray-level opening to avoid under prediction of the stored volume. We considered large puddles exceeding 20 cm^2 to counterbalance the effect of erroneous altitudes in the DEM. As on plot one most of the tracer solution was stored in large puddles in the compacted part, omitting small puddles does probably not change the results.

Compared to the soil surface, the puddles appeared smooth on the photographs. Therefore, we used the differences in image texture to identify their contours. Then, considering that the water surface is flat, the stored volume is the sum of the differences between the bottom

of puddles and the mean elevation of the borderline of puddles in the initial DEM (Mirzaei, 2008).

The calculation of stored volume was sensitive to the algorithm we used to identify puddles. Indeed, sometimes the contours of puddles were difficult to detect because of shadows of the cameras or the metallic frame supporting them. In this case the area of the puddle and therefore the stored volume were underestimated. Mirzaei (2008) showed in his work that water storage calculated using a DEM based on the same experimental device is lower compared to a laser meter, especially for rough surfaces. This is due to shadow effects of soil clods. However, he also reported that the surface covered by puddles was equally well estimated by stereophotography and laser meter. Because in our experiments the soil surfaces were rather smooth with one dominant depression on plot one, we assume that the DEMs and the surface covered by puddles were calculated reliably.

On plot two only small and flat puddles developed that could not be extracted by texture filters. One possible reason is that soil clods were still visible in the puddles and their surface appeared as rough as the surrounding soil. However, the stored volume was small compared to plot one and had therefore little influence on infiltration patterns. Puddle detection, volume and area calculations were implemented in HALCON (MVTec Software GmbH, Munich, Germany).

2.2.3 Stained soil profiles

We photographed the soil profiles in the lossless RAW-format (unprocessed data of the CCD camera sensor) and converted the images to JPEG after white balance adjustment in Photoshop CS2 (Adobe Systems Inc., San Jose, CA, USA) using the grey scales. Subsequently, we corrected the perspective and radial distortions by transforming the photographs such that they corresponded to images captured by an ideal camera that produced no radial distortion and that looked perpendicularly to the soil profile. Perspective transformation of the images was obtained via a homogenous transformation matrix (a matrix that combines information about both rotation and translation in one matrix) and radial distortion was modelled by:

$$\begin{pmatrix} u \\ v \end{pmatrix} = \frac{1}{1 + \kappa\,(\tilde{u}^2 + \tilde{v}^2)} \begin{pmatrix} \tilde{u} \\ \tilde{v} \end{pmatrix} \tag{1}$$

where the parameter κ is the magnitude of the radial distortion, $(\tilde{u}, \tilde{v})^T$ are coordinates of a point in the original image and $(u, v)^T$ are coordinates in the corrected one. If κ is negative, the distortion is barrel-shaped, while for positive κ it is pincushion-shaped (Steger et al., 2008).

Then we transformed the corrected images from RGB to HIS (hue, saturation, intensity) colour space and classified them in Brilliant Blue stained and non-stained areas. The change of colour space is necessary because the HIS colour space is more suitable for robust separation of colours independently of their intensities under varying illumination (MVTec Software GmbH, 2007). Subsequently, all grey values in an interval [low threshold, upper threshold] were classified as stained pixels. Misclassifications due for example to the shadow of the metallic frame were fixed manually. The correction of geometric distortion and classification of images were done in HALCON (MVTec Software GmbH, Munich, Germany). The classified photographs were converted to binary images (stained parts were coded black and non-stained

areas white) and used to calculate the dye coverage $p(d)$ (number of stained pixels in depth d) in MATLAB 7.1 (The MathWorks, Natick, MA, USA).

2.2.4 Analysis of flow patterns by extreme value statistics

Schlather and Huwe (2005) defined the form parameter ξ_r of the generalized Pareto distribution as a risk index for vulnerability of groundwater to pollutants. They fitted the distribution $1 - H$ to the dye coverage function $p(d)$ (number of stained pixels per depth), H being the *Generalized Pareto Distribution*:

$$H(d, \xi_r, s) = 1 - \left\{ 1 + \frac{\xi_r (d - d^*)}{s} \right\}^{\frac{1}{\xi_r}} \tag{2}$$

where d^* is the threshold depth beyond which the data are assumed to follow closely the Pareto distribution, d is the profile depth (d and d^* are measured in pixels on a photograph, $d > d^*$), ξ_r is the form parameter ($\xi_r \in \mathbb{R}$) and s is the scale parameter ($s > 0$), such that $(1 + \xi_r(d - d^*)/s) > 0$. According to Schlather and Huwe (2005) the dye coverage $p(d)$ is an estimate of the probability that a path is stained at least down to a depth d, modulo a constant factor m. The distribution $1 - H$ is fitted to the normalised dye coverage $p(d)/m$ and describes the conditional probability that a path is still stained to a depth d, given that it is stained to the depth d^* (for $d > d^*$).

Bogner et al. (2008) used the risk index ξ_r to analyse flow patterns in a forest soil. They advised to use the risk index together with the shape index and emphasized that it only describes flow processes in that particular part of the soil profile that was used for the fit. The authors proposed to combine the risk index with the shape parameter and to interpret the probability distribution $1 - H$ as a susceptibility of soils to vertical solute propagation.

We fitted the distribution $1 - H$ to the dye coverage of superposed profiles. They were calculated by summing all dye coverages of the respective experimental plot and normalizing them by the width of the profiles. The distribution $1 - H$ is the (conditional) probability to find the dye tracer in a certain depth and thus the susceptibility of the soil to vertical solute propagation. The goodness of fit was measured by the coefficient of determination R^2:

$$R^2 = 1 - \frac{\sum \left(p(d) - \hat{p}(d) \right)^2}{\sum \left(p(d) - \bar{p} \right)^2} \tag{3}$$

where $p(d)$ is the number of stained pixels in the depth d ($d > d^*$), $\hat{p}(d)$ is the estimated number of stained pixels in the depth d and $\bar{p}$ is the mean number of stained pixels in the part of the profile used for fitting the $1 - H$ distribution. The analysis was performed in R (R Development Core Team, 2008) using the add-on package SoPhy (Schlather, 2005).

3 Results and discussion

3.1 Initial conditions

The initial gravimetric soil moisture varied between 19 and 41% on plot one before the preliminary application of 54 mm of water and between 16 and 19% on plot two before tracer

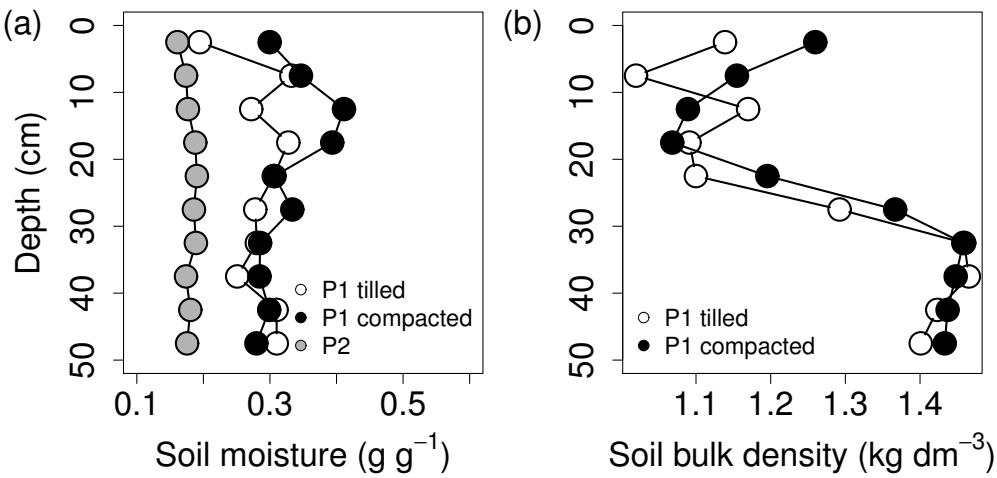

Figure 2: (a) Initial gravimetric soil moisture on plot one (P1) before the preliminary application of 56 mm of water and on plot two (P2); (b) soil bulk density of compacted and tilled parts of plot one (P1) measured by gamma ray attenuation.

application (Figure 2a). These differences reflected the natural variability in the field. Despite the preliminary irrigation on plot one, the initial volumetric water contents measured by the TDR probes in the soil matrix indicated similar moisture conditions on both plots before tracer application (Figure 3).

The soil bulk density profile reflected well the tillage. Indeed, it varied little in the top 20 cm that corresponded to the tilled part, increased rapidly in the tillage pan situated in about 25 cm depth and remained stable underneath. The multiple passage of the tractor wheel on plot one increased the soil bulk density in the top 10 cm (Figure 2b) compared to the tilled part. These results accord well with findings by Kulli et al. (2003) who reported a significant increase of the bulk density in the top 15 cm of the soil and in 55 cm depth after single and multiple passages of a sugar beet harvester. However, between 15 and 55 cm depth they found no significant differences.

3.2 Water storage and changes in soil microtopography

During the simulated rainfall large puddles occurred mainly in the compacted part of plot one. This indicates a decrease in infiltrability compared to the tilled part and accords well with results by Kulli et al. (2003). Indeed, they observed ponding during rainfall simulation studies on the surface of a trafficked plot and attributed it to soil compaction. The volume stored at the surface of plot one increased from 1.1 mm after 6 min of tracer application to 8.9 mm after 1 hour (Figure 4). The maximum area covered by large puddles was 29% after 1 hour of rainfall. However, the large volume stored at the soil surface is partly due to the metallic frame that surrounded the plot. Actually, the plot surface was inclined and the water backed up at the metallic frame. Therefore, the storage does not correspond to a natural situation, but would have contributed to the surface runoff. After the end of simulated rainfall the stored volume decreased rapidly.

Besides water storage, we observed translocation of soil particles on plot one. In fact,

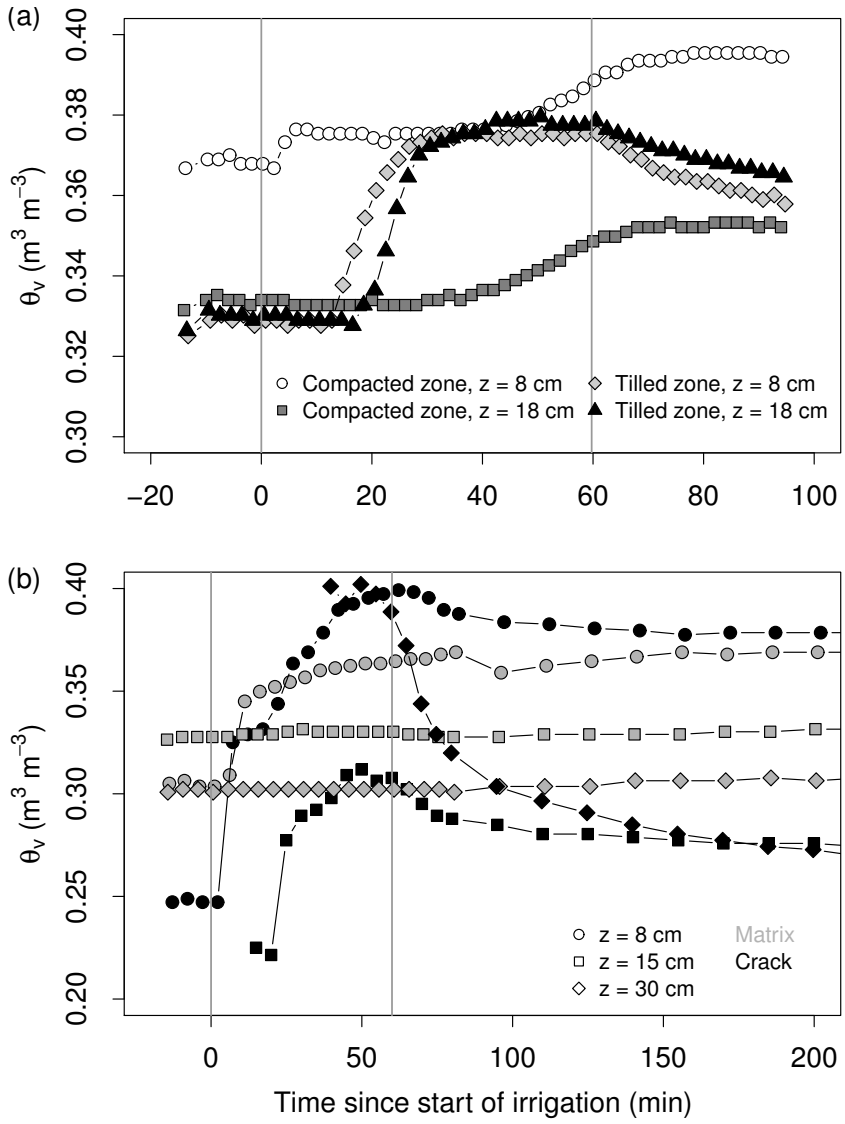

Figure 3: Volumetric water content in different depths during infiltration measured by TDR on plot one (a) and plot two (b). The grey-filled symbols in (b) belong to TDR sensors situated in the soil matrix and black-filled symbols indicate TDR measurements in a crack. The TDR probes installed at 8 and 15 cm depth are situated in the wall of a crack. In contrast, the TDR probe installed in 30 cm is placed at the bottom of a fissure inside loose soil material and captures the dynamics of water circulating inside the cracks. The vertical lines show the begin and the end of tracer application.

comparing the DEMs before and after rainfall simulation revealed that altitudes in the left part of the plot diminished and those in the right part (especially in the right lower corner) increased (Figure 5). This direction corresponds to the general slope of the plot. The median difference between the altitudes before and after tracer application was −0.9 mm, with a mean absolute deviation of 3.4 mm (5% and 95% quantiles equal −6.9 mm and 5.5 mm, respectively). On plot two, no similar large translocation patterns were visible because the plot was generally flat (Figure 5). However, small flat puddles appeared and local translocation/deposition took place. The median difference between the altitudes before and after the rainfall simulation equalled −0.8 mm, with a mean absolute deviation of 4.5 mm (5% and 95% quantiles equal −10.0 mm and 7.7 mm, respectively). Additionally, we observed a closing of cracks on the surface during tracer application.

The median differences between the altitudes before and after tracer application were small and similar on both plots. We attribute these mild changes to the low energy of the raindrops because their size and therefore their kinetic energy were small. On the other side, we actually observed flattening of soil clods and smoothing of the soil surface indicating the breakdown of soil aggregates. In their study, Le Bissonnais (1996) mentioned several possible mechanisms of breakdown of soil aggregates: slaking or breakdown by compression of trapped air, differential swelling, breakdown by mechanical impact of raindrops and dispersion. Due to their small size, the mechanical impact of the raindrops was probably low. Additionally, the large amount of clay might decrease the importance of slaking (Le Bissonnais, 1996). The macroscopic observations of the soil surface during the preliminary water application without tracer as well as during the tracer studies suggested dispersion as the main mechanism because of the small size of the resulting fragments (Le Bissonnais, 1996).

Dispersion is thought to decrease hydraulic conductivity and infiltration rate. However, its exact impact is not clear. Abu-Sharar and Salameh (1995), for instance, found in their study that dispersion has sometimes to be associated with slaking to reduce hydraulic conductivity. They attributed this to the small size of dispersed particles that despite their high mobility were not able to clog conducting macropores. During tracer application, dispersion might have increased because Brilliant Blue FCF contains sodium.

In our study, the effects of aggregate breakdown on the infiltration rate was possibly different on the two plots. On plot one, the compacted part (a depression) was probably most affected by sealing and crusting because there were no large macropores. Therefore, the infiltration rate might have decreased in this part. This accords well with findings by Bresson and Boiffin (1990) who reported that the occurrence of depositional crust, and thus deposition of soil particles, coincided with puddling. It was precisely in this part of the plot that the largest puddles were observed. Using the terminology by Bresson and Boiffin (1990), the large translocation of particles on plot one is related to the runoff–sedimentation regime. In contrast, local displacement of particles could be explained by a muddy flow process. Plot 2 and the tilled part of plot 1 were probably less affected by the decrease of the infiltration rate because of a larger macroporosity. This is in agreement with flow patterns described below.

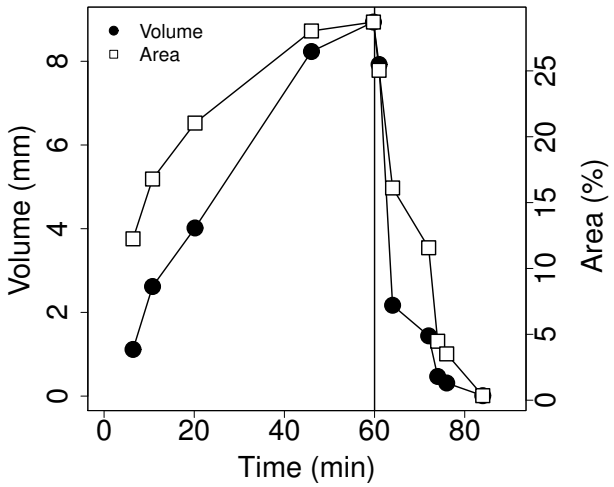

Figure 4: Volume stored on the soil surface during tracer application and area covered by puddles larger than 20 cm^2 on plot one. The vertical line indicates the end of tracer application. On plot two only small and flat puddles developed that could not be extracted by texture filters. However, the stored volume was small compared to plot one and had therefore little influence on infiltration patterns.

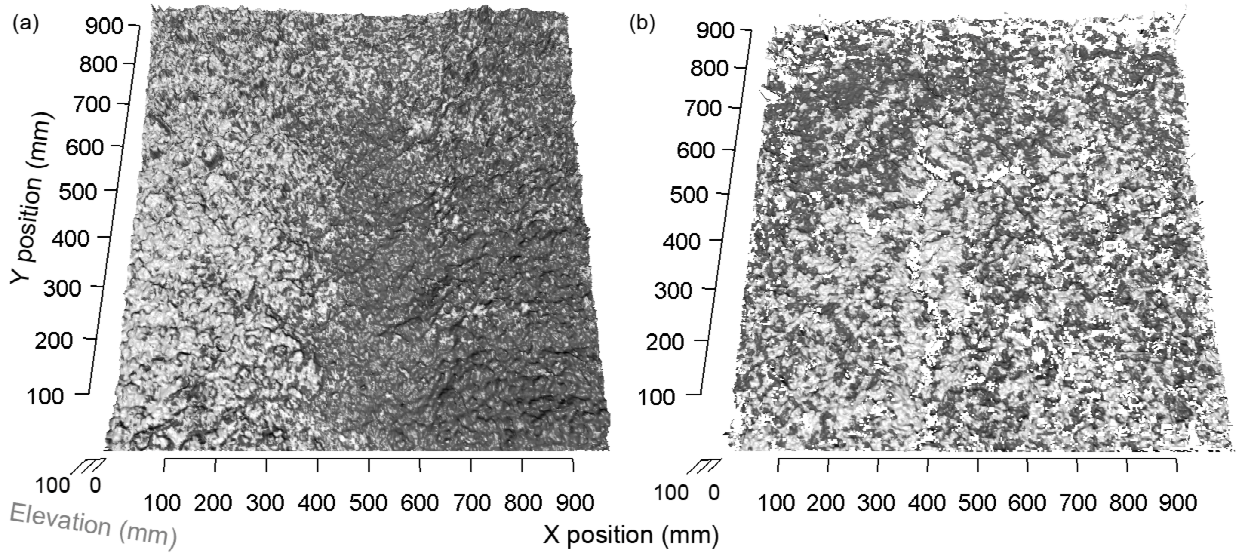

Figure 5: DEMs with patterns of particle translocation (light grey color) and particle deposition (dark grey color). White areas show missing values. (a) During the rainfall simulation on plot one soil particles were translocated from the left part to the right part of the plot deposited mostly in the lower right corner. This corresponds well with the general slope of the plot. (b) Plot two lacked such clear translocation patterns because it was generally flat.

3.3 Dynamics of soil water content

In the tilled zone of plot one, volumetric water content raised from 33 to 37% in 8 and 18 cm depth after about 10 min of rainfall (Figure 3a). Until the end of the tracer application it remained stable in 8 cm and increased slightly in 18 cm depth. After the end of irrigation the drainage was rapid, especially in 8 cm depth. This fast increase in soil moisture as well as its quick decrease indicate the occurrence of preferential flow probably through inter-aggregate voids created by tillage.

TDR probes situated in the compacted zone recorded a totally different dynamics. There, the volumetric water content raised slowly and the relative increase was smaller than in the tilled part. However, this shows that the compacted zone was not completely bypassed by the flow. The offset recorded at the beginning of irrigation in 8 cm depth is probably an artefact. The soil moisture continued to increase after the end of tracer application, possibly due to the infiltration of water stored in large puddles or because of lateral redistribution.

On plot two, TDR probes in 8 cm depth situated in fissures and in the soil matrix responded 7 min after the start of irrigation (Figure 3b). Deeper in the soil, however, the soil water content remained stable in the soil matrix during and after the end of the experiment. In contrast, it raised quickly after the onset of irrigation and decreased after the end of simulated rainfall in fissures. This phenomenon was particularly pronounced in 30 cm depth.

In summary, the TDR probes showed a slow infiltration into the soil matrix characterised by a low conductivity because of a high clay content (Table 1). Inside the soil fissures, we observed a rapid water flow up to a depth of 30 cm, followed by a rapid drainage after the end of simulated rainfall. This corresponds to a preferential infiltration along soil fissures and to a rapid drainage of macropores. Indeed, the TDR probe installed at 30 cm depth is placed at the bottom of a fissure inside loose soil material and captures the dynamics of water circulating inside the cracks. The TDR probes installed at 8 and 15 cm depth are situated in the wall of a crack. They indicate that water flowing inside the fissures increases the soil moisture in its vicinity (i.e. infiltrates laterally into the soil matrix).

3.4 Flow patterns

The measurements of TDR probes accorded well with the heterogeneous dye patterns (Figure 6). On plot one two distinct zones could be identified: large stained areas above the plough pan (situated in about 25 cm depth) and narrow stained objects below it. In the tilled part water flowed preferentially through inter-aggregate spaces created by tillage. However, the large dye coverage in the upper part of this plot indicated a spreading of the dye into the soil matrix. This observation is in agreement with Schwartz et al. (1999) who reported that tillage increased the interaction of the dye with the soil matrix. The compacted zone is clearly visible and characterised by a shallower infiltration, nevertheless it was not completely bypassed by the flow (Figure 6a). Above the plough pan, the amount of stained area varied considerably more than below. Additionally, we observed a lateral funnelling of the tracer solution along the plough pan.

Although the plough pan constituted a discontinuity for the water flow, macropores situated underneath conducted water. This is in accordance with Logsdon (1995) who found in column studies that buried macropores below the tilled layer were not harmed and could

function as preferential flow pathways. However, their study was done on filled soil columns with an artificial macropore. In contrast, Capowiez et al. (2009) showed under field conditions that biomacropores, in that case earthworm burrows, still functioned under the tillage pan.

Compared to plot one, on plot two no visible plough pan was detected and cracks continued from soil surface down to the subsoil. The top 5 cm of the soil were homogenously stained indicating the dominance of the matrix flow. Below, the flow was funnelled to the fissures where the tracer was transported predominantly. Indeed, due to low permeability of the soil matrix lateral spreading of the tracer from preferential pathways into the matrix was low. This resulted in narrow stained objects ranging from the top to the bottom of the soil profiles (Figure 6b). As described by Jarvis (2007) and the references given therein, for large macropores to conduct water flow water pressures must reach close to saturation (> -10 cm). It does not mean that the entire soil profile must wet up. Near-saturation conditions need only occur locally (e.g. in millimetre thick layers around fissures or above compacted soil zones like plough pans).

3.5 Effects of tillage and compaction on flow patterns

Agricultural cropping systems are highly dynamic and characterised by frequent disturbances of the soil surface by tillage and compaction. Our results showed that compaction led to an increase of soil bulk density and thus might decrease the macroporosity. The compacted region on plot one was partly bypassed by the tracer and was prone to puddling. Sealing and crusting of the surface could have contributed to a decrease of the infiltration rate, especially in this part of the plot.

Furthermore, tillage led to a partial disconnection of transport processes above the plough pan from those underneath because macropores were disrupted and buried by the tillage operation. However, cracks underneath the plough pan remained stable and still functioned as preferential flow paths. Compaction clearly reduced the infiltration of the tracer. Nevertheless, due to the funnelling of flow along the tillage pan, macropores situated directly below the compacted part also participated in water flow.

3.6 Susceptibility of the soil to vertical solute propagation

On plot one, the amount of tracer infiltrated into the subsoil was smaller than on plot two. This was clearly reflected by the dye coverages (Figure 6) that showed a larger stained area in the subsoil on plot two than on plot one. Additionally, the more intense staining (not shown) of the subsoil on plot two evidenced a larger amount of infiltrated tracer. The plough pan was well visible in the dye coverage of superposed profiles of plot one and highlighted the slope change in about 25 cm depth (Figure 7).

As indicated by the fitted distribution $1 - H$, the susceptibility of the soil to vertical solute propagation was higher on plot two where the plough pan did not disrupt the continuity of fissures. This means that the studied soil is susceptible to deep vertical solute propagation when fissures are open and connected from the soil surface down to the subsoil. However, on both plots the probability to find the tracer at the bottom of the soil profiles (in approximately 1 m depth) was larger than zero (Table 2). This result showed that tillage and compaction did not prevent preferential flow in the subsoil by destroying macropores in the upper soil.

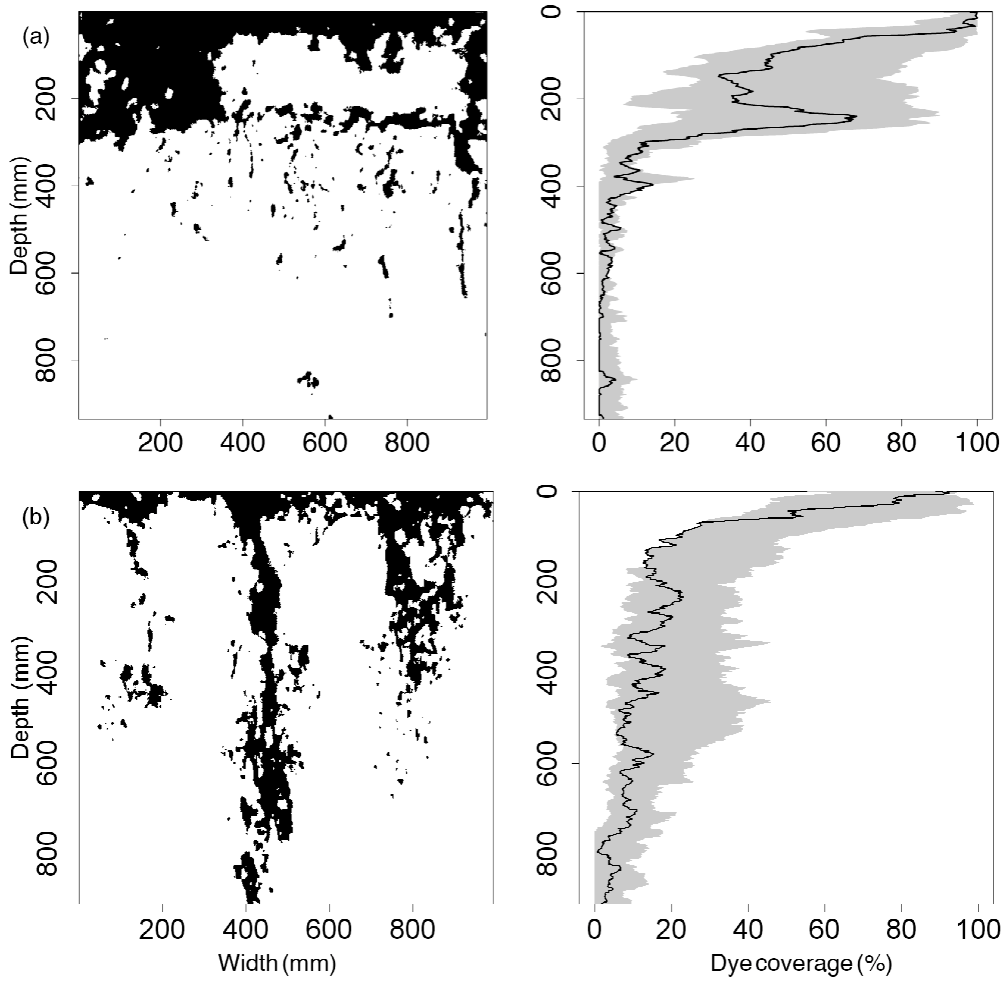

Figure 6: The left column shows example images of stained patterns: (a) plot one with the compacted part between 300 and 700 mm; (b) plot two. The compacted part on plot one was partly bypassed by the flow. Additionally, the tillage pan is clearly visible by lateral funnelling of tracer solution. Although the plough pan constituted a discontinuity for the water flow, macropores below the plough pan conducted water. In contrast, on plot two no visible plough pan was detected and cracks continued from soil surface down to the subsoil. The right column contains the dye coverages (black solid line) of the example images with the grey area indicating the minimum and maximum dye coverage of all stained profiles. For coloured photographs of the stained soil profiles see supplementary online material.

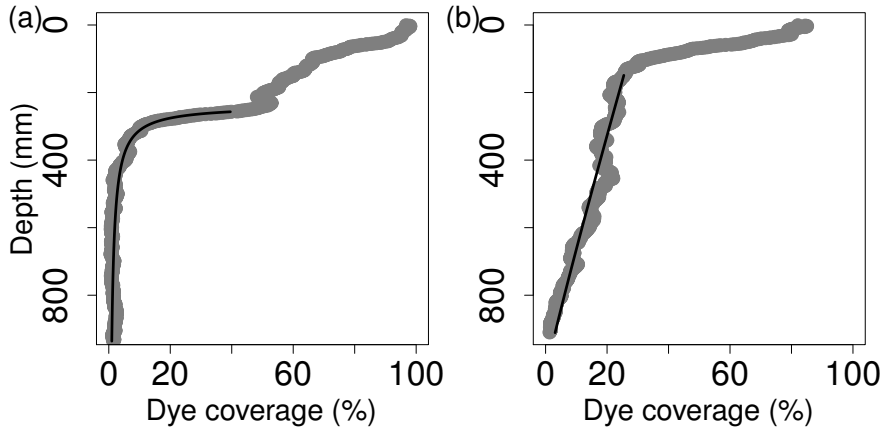

Figure 7: Dye coverage functions of superposed profiles (grey line) on plot one (a) and plot two (b). The black line shows the fitted distribution $1 - H$. The distribution was fitted from the depth beyond which the data are assumed to follow closely the Pareto distribution.

Table 2: The fitted parameters of the $1 - H$ distribution.

Plot	ξ_r	s	R^2	$1 - H(\%)^{\text{a}}$
I	0.96	18	0.97	1
II	−0.93	827	0.93	3

[a] Probability to find the tracer at the bottom of the profile in ca. 1 m depth.

The susceptibility of the studies soil to deep vertical solute propagation varies with time. Indeed, after dry periods and at no-till conditions, infiltration at our study site seems to be dominated by macropore flow through open cracks. Under such conditions, solute transport from the soil surface to the topsoil and down to the subsoil takes place. On the other hand, previous studies conducted at this site showed that during moister periods and at no-till conditions cracks in the upper soil were closed and macroporosity reduced. In this case matrix flow dominates and Brilliant Blue does not penetrate into the subsoil (Bogner, unpublished data).

4 Conclusions

Stereo photogrammetry is a useful technique to detect changes in microtopography and allows to monitor particle translocation and deposition during rainfall. However, it is important to carefully illuminate the surface to avoid shading by the apparatus and by soil clods as far as possible.

At our study site, cracks were dominant transport paths below the tillage pan, irrespective of tillage or compaction of the soil surface. Indeed, cracks buried after tillage still conducted the tracer solution and the dye penetrated in 1 m depth on the non-tilled as well as on the

tilled plot. However, the amount of the dye transported down to the subsoil was larger on the non-tilled plot with open cracks.

Compaction destroyed macroporosity in the topsoil and tillage disconnected it at the tillage pan from the subsoil, thus reducing the amount of solutes infiltrating into greater depths. However, our results clearly show that tillage and compaction do not necessarily prevent macropore flow. Therefore, we conclude that the studied soil is susceptible to deep vertical solute propagation especially at dry conditions when cracks are open and connected from the soil surface down to the subsoil.

Acknowledgements

The authors are grateful to the technical stuff of INRA Avignon for their help during field work and to Prof. M. Schlather for assistance in data analysis. The first author was financially supported by the Deutsche Forschungsgemeinschaft (DFG FOR 562) and the Deutsch-Französische Hochschule (Grant N° CT-31-06). We thank the anonymous reviewers for their valuable comments that helped to improve the manuscript.

References

Abu-Sharar T and Salameh A. 1995. Reductions in hydraulic conductivity and infiltration rate in relation to aggregate stability and irrigation water turbidity. *Agricultural Water Management*, **29** 53–62.

Alakukku L. 1996a. Persistence of soil compaction due to high axle load traffic. i. short-term effects on the properties of clay and organic soils. *Soil and Tillage Research*, **37**(4): 211–222.

Alakukku L. 1996b. Persistence of soil compaction due to high axle load traffic. ii. long-term effects on the properties of fine-textured and organic soils. *Soil and Tillage Research*, **37**(4): 223–238.

Bogner C, Wolf B, Schlather M, and Huwe B. 2008. Analysing flow patterns from dye tracer experiments in a forest soil using extreme value statistics. *European Journal of Soil Science*, **59**(1): 103–113.

Bresson LM and Boiffin J. 1990. Morphological characterization of soil crust development stages on an experimental field. *Geoderma*, **47** 301–325.

Capowiez Y, Cadoux S, Bouchant P, Ruy S, Roger-Estrade J, Richard G, and Boizard H. 2009. The effect of tillage type and cropping system on earthworm communities, macroporosity and water infiltration. *Soil and Tillage Research*, **105**(2): 209–216.

Flury M and Flühler H. 1994. Brilliant Blue FCF as a dye tracer for solute transport studies - a toxicological overview. *Journal of Environmental Quality*, **23**(5): 1108–1112.

Flury M, Flühler H, Jury WA, and Leuenberger J. 1994. Susceptibility of soils to preferential flow of water: a field study. *Water Resources Research*, **30**(7): 1945–1954.

German-Heins J and Flury M. 2000. Sorption of brilliant blue fcf in soils as affected by ph and ionic strength. *Geoderma*, **97**(1-2): 87–101.

Ghodrati M and Jury WA. 1992. A field-study of the effects of soil structure and irrigation method on preferential flow of pesticides in unsaturated soil. *Journal of Contaminant Hydrology*, **11**(1-2): 101–125.

Ghodrati M, Ernst FF, and Jury WA. 1990. Automated spray system for application of solutes to small field plots. *Soil Science Society of America Journal*, **54**(1): 287–290.

Hairsine PB, Moran CJ, and Rose CW. 1992. Recent developments regarding the influence of soil surface characteristics on overland flow and erosion. *Australian Journal of Soil Research*, **30** 249–264.

Håkansson I and Reeder RC. 1994. Subsoil compaction by vehicles with high axle load–extent, persistence and crop response. *Soil and Tillage Research*, **29**(2-3): 277–304.

Hansen B, Schjønning P, and Sibbesen E. 1999. Roughness indices for estimation of depression storage capacity of tilled soil surfaces. *Soil and Tillage Research*, **52**(1-2): 103–111.

Hendrickx JMH and Flury M. 2001. Uniform and preferential flow mechanisms in the vadose zone. In Council NR, editor, *Conceptual Models of Flow and Transport in the Fractured Vadose Zone*, pages 149–187. National Academy Press, Washington, DC.

Huang CH. 1998. Quantification of soil microtopography and surface roughness. In Baveye P, Parlange JY, and Stewart B, editors, *Fractals in Soil Science*, Advances in Soil Science. CRC Press Boca Raton, Florida.

IUSS Working Group WRB. 2007. World reference base for soil resources 2006, first update 2007. World Soil Resources Reports No. 103. http://www.fao.org/ag/agl/agll/wrb/doc/wrb2007_corr.pdf. [Accessed on 6-August-2011].

Jarvis NJ. 2007. A review of non-equilibrium water flow and solute transport in soil macropores: principles, controlling factors and consequences for water quality. *European Journal of Soil Science*, **58**(3): 523–546.

Jeffery GH, Bassett J, Mendham J, and Denney RC, editors. 1989. *Vogel's textbook of quantitative chemical analysis*. Prentice Hall, 5th edition.

Jeschke W. 1990. Digital close-range photogrammetry for surface measurement. In Gruen A and Bellingham EPB, editors, *Close-Range Photogrammetry Meets Machine Vision, SPIE Proceedings*, volume 1395. WA: Society for Photo-Optical Instrumentation Engineers.

Jester W and Klik A. 2005. Soil surface roughness measurement - methods, applicability, and surface representation. *Catena*, **64**(2-3): 174–192.

Ketelsen H and Meyer-Windel S. 1999. Adsorption of Brilliant Blue FCF by soils. *Geoderma*, **90**(1-2): 131–145.

Kulli B, Gysi M, and Flühler H. 2003. Visualizing soil compaction based on flow pattern analysis. *Soil and Tillage Research*, **70**(1): 29–40.

Le Bissonnais Y. 1996. Aggregate stability and assessment of soil crustability and erodibility: I. theory and methodology. *European Journal of Soil Science*, **47** 425–437.

Logsdon SD. 1995. Flow mechanisms through continuous and buried macropores. *Soil Science*, **160**(4): 237–242.

Lu J and Wu L. 2003. Visualizing bromide and iodide water tracer in soil profiles by spray methods. *Journal of Environmental Quality*, **32**(1): 363–367.

Mirzaei MR. 2008. *Effet de la variabilité spatiale des états de surface du sol sur le partage infiltration-ruissellement: Caractérisation expérimentale par photogrammétrie et modélisation*. Ph.d. thesis, University of Avignon, France. In French.

Mooney S and Nipattasuk W. 2003. Quantification of the effects of soil compaction on water flow using dye tracers and image analysis. *Soil Use and Management*, **19**(4): 356–363.

Moreno RG, Alvarez MCD, Requejo AS, and Tarquis AM. 2008. Multifractal analysis of soil surface roughness. *Vadose Zone Journal*, **7**(2): 512–520.

MVTec Software GmbH. 2007. Solution Guide I. Basics.

Paz-Ferreiro J, Bertol I, and Vazquez E. 2008. Quantification of tillage, plant cover, and cumulative rainfall effects on soil surface microrelief by statistical, geostatistical and fractal indices. *Nonlinear Processes in Geophysics*, **15**(4): 575–590.

Pickering NB, Richard TL, Parlange JY, Waltman WJ, and Kromm L. 1988. Dye tracer analysis of preferential flow to groundwater. Department of agricultural and biological engineering, staff report 88-2, Cornell University, Ithaca, N. Y.

R Development Core Team. 2008. R: A language and environment for statistical computing.

Schlather M. 2005. SoPhy: some soil physics tools for R, ver. 1.0.39.

Schlather M and Huwe B. 2005. A risk index for characterising flow pattern in soils using dye tracer distributions. *Journal of Contaminant Hydrology*, **79**(1-2): 25–44.

Schwartz RC, McInnes KJ, Juo ASR, and Cervantes CE. 1999. The vertical distribution of a dye tracer in a layered soil. *Soil Science*, **164**(8): 561–573.

Steger C, Ulrich M, and Wiedemann C. 2008. *Machine Vision Algorithms and Applications*. Wiley-VCH.

Strudley MW, Green TR, and Ascough JC, III. 2008. Tillage effects on soil hydraulic properties in space and time: State of the science. *Soil and Tillage Research*, **99**(1): 4–48.

Taconet O and Ciarletti V. 2007. Estimating soil roughness indices on a ridge-and-furrow surface using stereo photogrammetry. *Soil and Tillage Research*, **93**(1): 64–76.

Tebrugge F and During R. 1999. Reducing tillage intensity - a review of results from a long-term study in Germany. *Soil and Tillage Research*, **53**(1): 15–28.

Vervoort RW, Radcliffe DE, and West LT. 1999. Soil structure development and preferential solute flow. *Water Resources Research*, **35**(4): 913–928.

Vidal Vàzquez EV, Miranda JGV, Alves MC, and Paz González A. 2006. Effect of tillage on fractal indices describing soil surface microrelief of a brazilian alfisol. *Geoderma*, **134**(3-4): 428–439.

Warner WS. 1995. Mapping a 3-dimensional soil surface with hand-held 35 mm photography. *Soil and Tillage Research*, **34**(3): 187–197.